# Nanofiltration across Defect-Sealed Nanoporous Monolayer Graphene

Sean C. O'Hern,[†] Doojoon Jang,[†] Suman Bose,[†] Juan-Carlos Idrobo,[‡] Yi Song,[§] Tahar Laoui,[∥] Jing Kong,[§] and Rohit Karnik*,[†]

[†]Department of Mechanical Engineering, Massachusetts Institute of Technology, Cambridge, Massachusetts 02139, United States
[‡]Center for Nanophase Materials Sciences, Oak Ridge National Laboratory, Oak Ridge, Tennessee 37831, United States
[§]Department of Electrical Engineering and Computer Science, Massachusetts Institute of Technology, Cambridge, Massachusetts 02139, United States
[∥]Department of Mechanical Engineering, King Fahd University of Petroleum and Minerals, Dhahran 31261, Saudi Arabia

Ⓢ Supporting Information

**ABSTRACT:** Monolayer nanoporous graphene represents an ideal membrane for molecular separations, but its practical realization is impeded by leakage through defects in the ultrathin graphene. Here, we report a multiscale leakage—sealing process that exploits the nonpolar nature and impermeability of pristine graphene to selectively block defects, resulting in a centimeter-scale membrane that can separate two fluid reservoirs by an atomically thin layer of graphene. After introducing subnanometer pores in graphene, the membrane exhibited rejection of multivalent ions and small molecules and water flux consistent with prior molecular dynamics simulations. The results indicate the feasibility of constructing defect-tolerant monolayer graphene membranes for nanofiltration, desalination, and other separation processes.

**KEYWORDS:** Molecular sieve, filter, membrane, desalination, reverse osmosis, forward osmosis
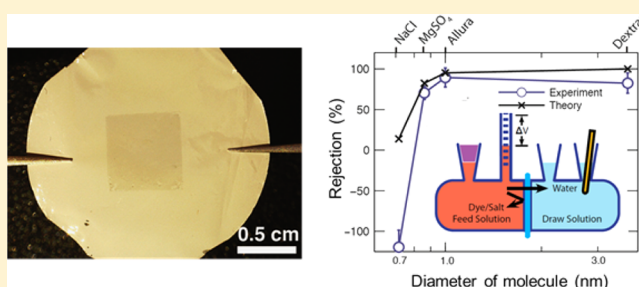
Decreasing water supplies driven by an increasing population, climate change, and industrialization demands the development of new technologies that reduce the costs of water production to meet future needs.[1,2] Graphene, a single sheet of carbon atoms, may provide the foundation for a new class of highly permeable membranes for water purification and desalination.[3−6] Though atomically thin, graphene in its pristine form exhibits both exceptional mechanical strength[7] and imperviousness to atoms as small as helium.[8] Nanoporous graphene with a high density of subnanometer pores is predicted to allow ultrafast water permeance and high salt rejection because the atomic thinness provides little resistance to flow, yet blocks the passage of solutes that are larger than the pores.[4,9−11]

Ideally, graphene would contain only uniformly sized pores at high density, but intrinsic defects from the growth process and extrinsic defects from graphene transfer[12−14] form leakage pathways that make practical realization of graphene membranes extremely challenging. Despite remarkable advances including high-density pore creation,[13] gas selectivity across micrometer-sized graphene,[15] and membranes with large (>5 nm) pores,[16] filtration of salts and small molecules across monolayer graphene—which necessitates nanometer or subnanometer pores to achieve the required selectivity—has remained elusive due to its high susceptibility to leakage.

Despite manufacturing advances,[17] complete elimination of defects is improbable. Therefore, sealing, blocking, or reducing molecular permeation through defects is paramount to the practical realization of molecular-level filtration across nanoporous graphene. Here, we demonstrate nanofiltration of salts and small molecules across centimeter-scale nanoporous monolayer graphene enabled by a multiscale process to seal defects while leaving a significant fraction of monolayer graphene usable as the active separation material.

To fabricate a graphene membrane, we transferred graphene grown on copper foil to a polycarbonate track etch (PCTE) membrane with 200 nm pores that provides mechanical support (see Supporting Information).[12−14] Mass transport measurements and electron microscopy show that this composite membrane contains nanometer-scale (~1−15 nm) intrinsic defects formed during chemical vapor deposition of graphene on copper, and large (~100−200 nm) tears generated during graphene transfer.[14] This broad distribution of defects required a two-step multiscale sealing procedure. First, nanometer-sized intrinsic defects were sealed by selectively filling with hafnia using atomic layer deposition (ALD).
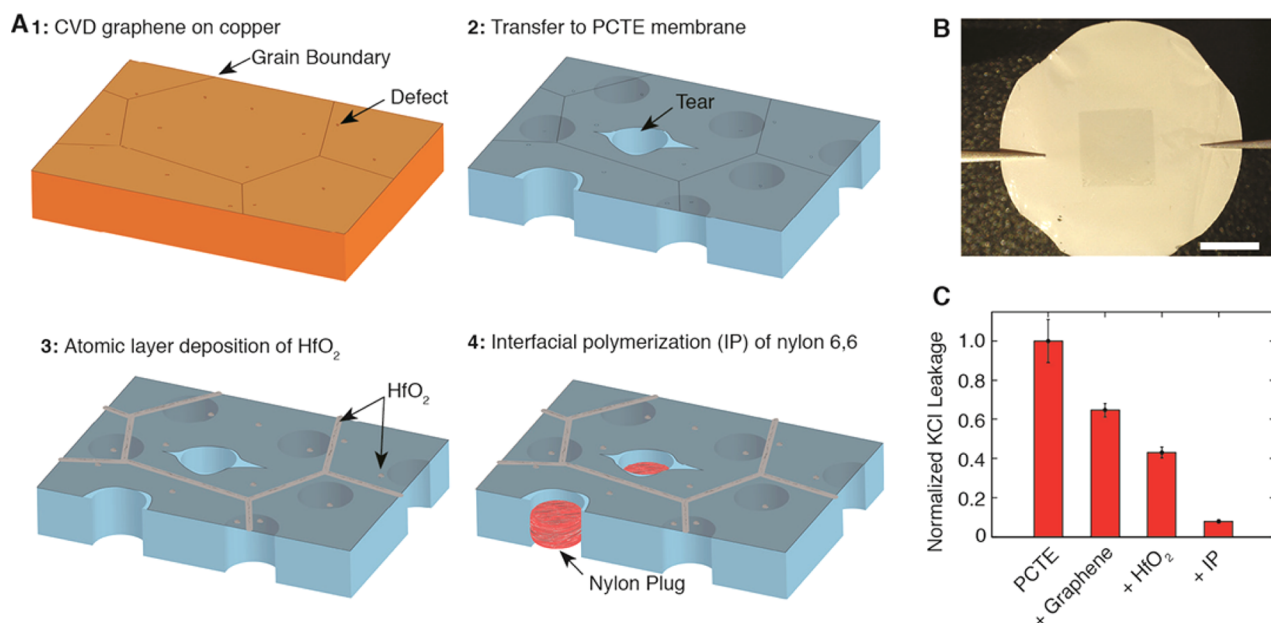
**Figure 1.** Graphene membrane fabrication and defect-sealing procedure. (A) (1) CVD graphene on copper substrate, containing grain boundaries and pinhole defects, is transferred to a polycarbonate track etch (PCTE) membrane (2) by first pressing the graphene-on-copper onto the PCTE membrane and subsequently etching away the copper. After transfer, the graphene membrane contains the intrinsic defects and grain boundaries as well as fabrication defects such as tears unintentionally introduced during transfer. (3) To seal nanoscale defects and leaks, ∼3.5 nm of hafnia is deposited onto the graphene surface using atomic layer deposition (ALD) to selectively cover grain boundaries and seal nanometer-sized intrinsic defects. (4) Next, nylon-6,6 is formed in PCTE pores underlying larger defects via interfacial polymerization (IP). (B) Photograph of final membrane with the graphene layer visible at the center of the PCTE membrane. Scale bar is 0.5 cm. (C) Diffusive transport of potassium chloride (KCl) through the control membranes (no pores created) normalized by transport rate through a bare PCTE membrane decreases with each successive sealing step, with a final leakage rate of ∼8%. Error bars represent 95% confidence interval of three measurements on a single membrane.
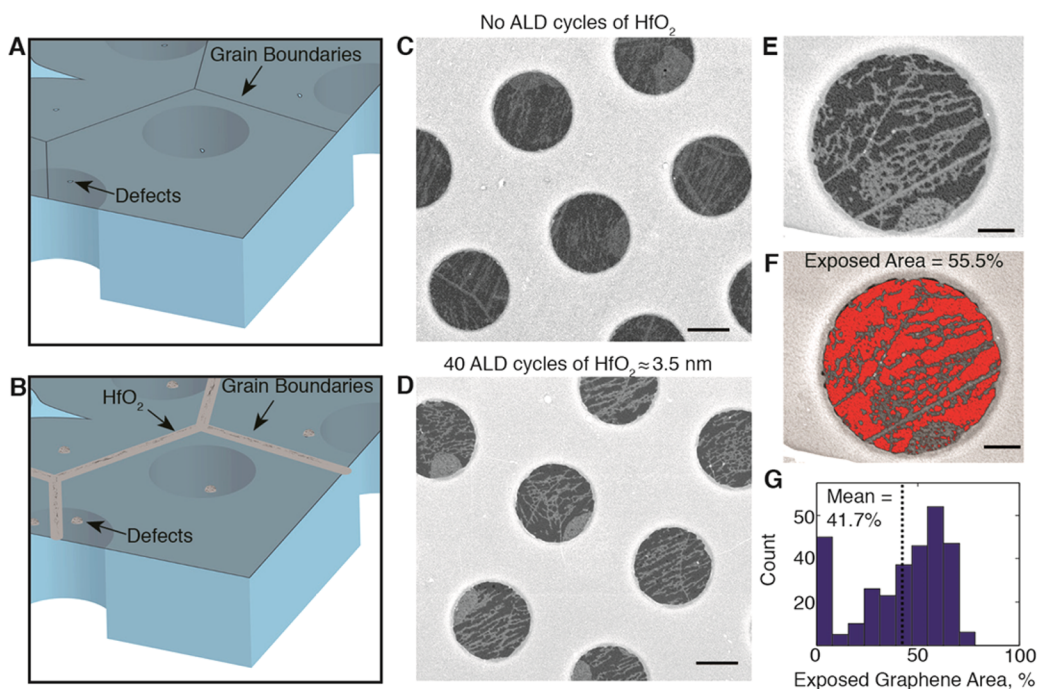


**Figure 2.** Atomic layer deposition (ALD) of hafnia (HfO$_2$) to cover intrinsic defects. (A) The graphene membrane contains grain boundaries and intrinsic defects that permit leakage transport to bypass controlled, subnanometer pores. (B) ALD precursors selectively adsorb on defects and grain boundaries but not on the basal plane, thereby sealing small undesirable pores in the graphene membrane. Graphene suspended over pores of an electron microscopy grid without (C) and with (D−E) hafnia deposition demonstrates selective coverage over defects, grain boundaries, and surface contamination, as imaged by scanning electron microscopy (SEM). Scale bars are 500 nm in (C−D) and 200 nm in (E). (F) Analysis of a single suspended graphene membrane with 55.5% area of uncovered graphene (not coated with hafnia), indicated in red color. Scale bar is 200 nm. (G) Histogram of the number of suspended graphene membranes with a given fraction of uncovered graphene demonstrates that on average 41.7% of the graphene remains uncovered by hafnia.
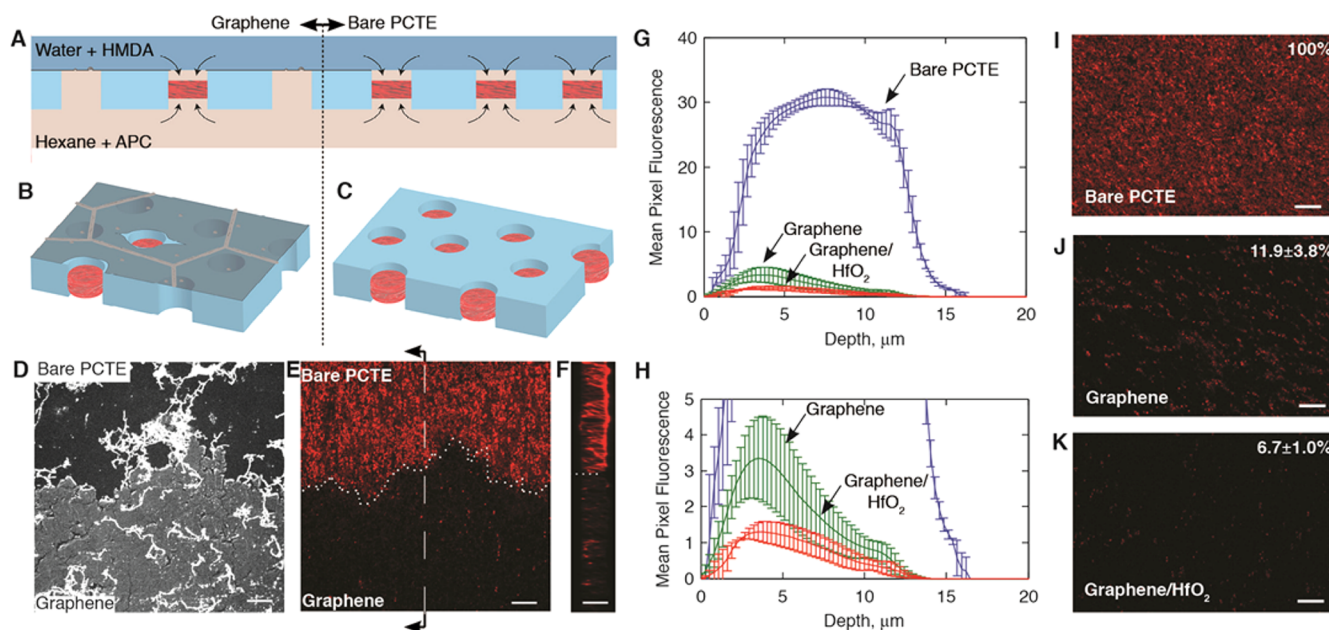
**Figure 3.** Interfacial polymerization (IP) to block large defects in graphene. (A) The process exploits the impermeabiliy of graphene by placing the membrane at the interface of aqueous hexamethylenediamine (HMDA) and adipoyl chloride (APC) in hexane. (B) Nylon-6,6 (red) is formed behind large defects in the graphene where HMDA can diffuse into the organic phase and react with APC. (C) However, in the absence of graphene, nylon forms in all PCTE pores. (D−F) Reflected light and confocal fluorescence images of fluorescently labeled nylon formed in a PCTE membrane partly covered with graphene (light area in (D)) reveals that nylon (red color in (E)) is observed prominently only where graphene does not cover the PCTE membrane. (G−H) The distribution of averaged fluorescence signal across the depth of the membrane (z dimension of the confocal image) indicates uniform formation of nylon throughout the membrane thickness. Behind graphene or graphene coated with hafnia, nylon formation is minimal and shifted toward the graphene side. (I−K) Fluorescence images of PCTE membrane without graphene, with graphene, and with hafnia-coated graphene show successively lower formation of nylon. The volume-averaged fluorescence intensity normalized by that of the bare PCTE membrane is indicated in the upper right corner. Scale bars are 10 $\mu$m on all panels. Error bars represent standard deviation of mean pixel fluorescence measurements from three different sections of the same membrane.

Second, the large defects were sealed via an interfacial polymerization reaction that exploited the impermeability of graphene to achieve selective blocking of defect sites (Figure 1A). We characterized this leakage−sealing process using diffusion of potassium chloride across the membrane[14] (Figure 1B−C and Supporting Information Figure S1). Transferring a monolayer of graphene to a PCTE membrane decreased the flux of potassium chloride to ∼65% of that across a PCTE membrane without graphene. Ideally, transferring a defect-free monolayer of graphene to a PCTE membrane would decrease the flux to zero; therefore, the measured flux corresponds to leakage across the graphene layer. Deposition of hafnia on graphene decreased the flux to ∼40%, and subsequent interfacial polymerization further decreased it to ∼8% of that across a PCTE membrane without graphene. This decrease in flux demonstrates the ability to decrease leakage across defects in the graphene layer.

The ALD sealing process exploits the increased surface energy at graphene defects to preferentially adsorb the gas precursor molecules during deposition of metal oxides.[19] Metal oxide deposition starts at grain boundaries, point defects, contamination, wrinkles, and edges and then proceeds laterally across the surface.[19] This phenomenon makes it difficult to apply dielectric coatings to suspended graphene using ALD, but here we exploit it to seal defects (Figure 2A−B). We use ALD of hafnia because it resists dissolution in acidic and basic solutions[20] (Supporting Information Figure S4) and find that deposition of a 3.5 nm-thick film on suspended graphene leaves a significant area free of hafnia. Scanning electron microscopy (SEM) reveals that the deposited hafnia closely follows

wrinkles and contamination on graphene (Figure 2C−D). Quantitative image analysis shows that ∼42% of the suspended graphene is available for use as an ultrathin membrane (Figure 2E−G). Additional cycles of hafnia may reduce leakage, but it is at the expense of further reduction in the active graphene area.

The interfacial polymerization process to seal larger defects exploits the impermeability of graphene[8] to block a polycondensation reaction between two monomers introduced on either side of the membrane. We introduced aqueous hexamethylenediamine from the graphene side and an organic solution of adipoyl chloride on the PCTE membrane side to deposit nylon-6,6 where the two monomers come into contact (Figure 3).[21,22] Due to the solubility of hexamethylenediamine in the organic phase, nylon-6,6 forms within the organic phase where the mass fluxes of the two monomers result in the correct stoichiometry.[22] Because the PCTE membrane pores are wetted by the organic phase, we expect nylon-6,6 to deposit within the PCTE pores behind large graphene defects that are not sealed using ALD (Figure 3). Confocal fluorescence microscopy using fluorescently labeled polymer revealed that covering a PCTE membrane with graphene and hafnia-coated graphene reduced the occurrence of polymer formation by ∼88% and ∼93%, respectively, compared to a bare PCTE membrane, while simultaneously altering the distribution of the polymer across the membrane cross-section (Figure 3D−K). The dramatic decrease in polymer formation below monolayer graphene (Figure 3D-E) confirms its impermeability and agrees with the measured coverage of graphene on PCTE membranes.[14] The additional decrease in polymer formation after hafnia deposition (Figure 3J−K) further confirms the
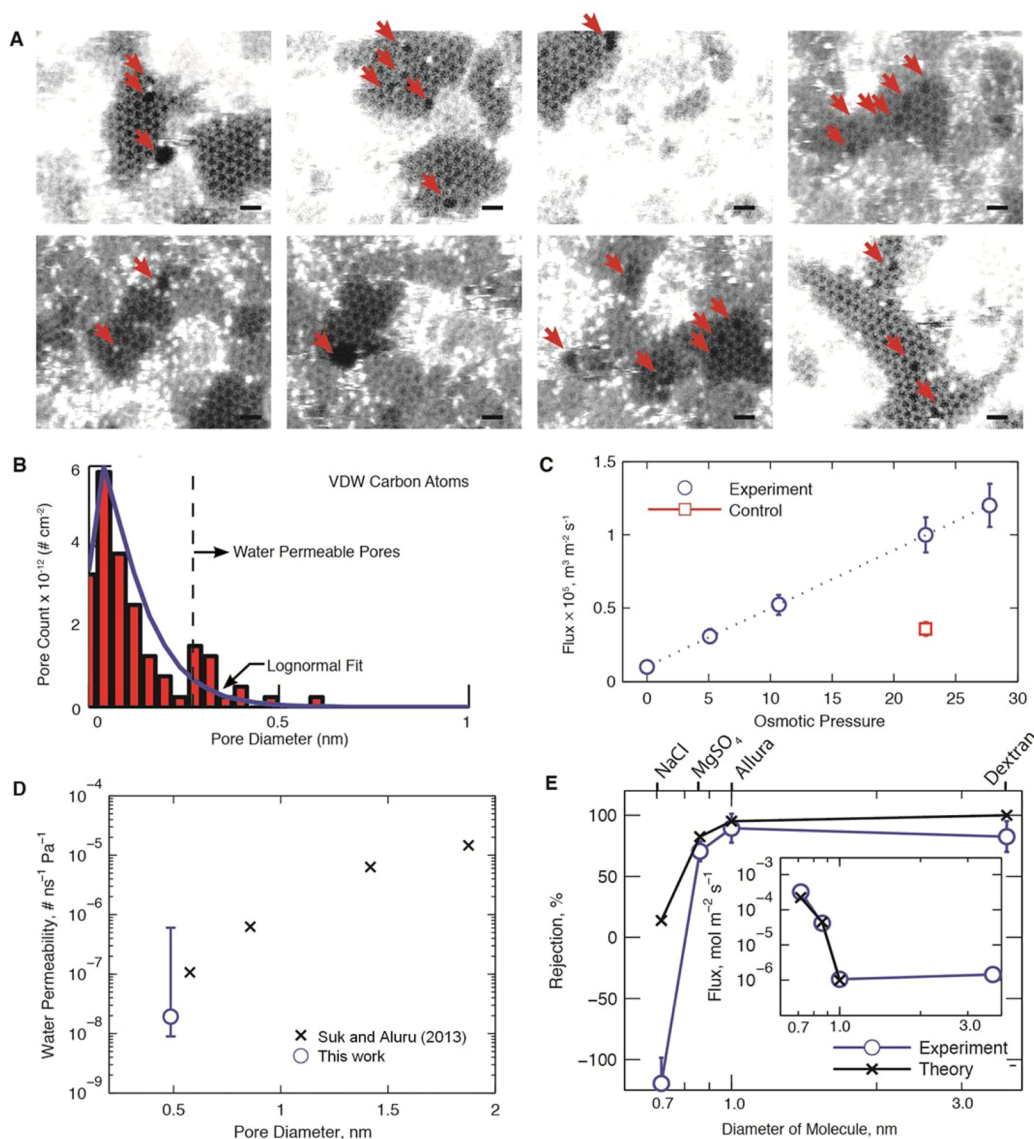
**Figure 4.** Water transport and filtration across nanoporous graphene. (A) Examples of pores created in graphene membrane through ion bombardment followed by chemical oxidation. Images were obtained using aberration-corrected scanning transmission electron microscopy (STEM) and processed as described in the online Supporting Information. Scale bars are 0.5 nm in all panels. (B) Distribution of measured pore diameters adjusted to the van der Waals diameter of carbon atoms. Pores larger than 0.275 nm in diameter are expected to be water permeable. (C) Water flux through nanoporous graphene membrane compared to control membrane without ion bombardment. In nanoporous graphene, water flux is linearly proportional to osmotic pressure. In the control, water permeates across defects. (D) Experimentally measured water permeability per graphene nanopore agrees well with molecular dynamics simulations by Suk and Aluru.[10] (E) Experimentally measured rejection and molar flux (inset) of solutes agrees well with the theoretical continuum model (see Supporting Information section III.E), except in the case of NaCl due to additional leakage pathways. Error bars represent 95% confidence in (C) and (E) and estimated bounds in (D) (see Supporting Information III.D for details).

efficacy of the ALD process to seal intrinsic defects. When nylon forms behind a graphene-coated PCTE pore, its position is shifted toward the graphene side (Figure 3G−H). This shift is consistent with residual defects in graphene hindering the transport of hexamethylenediamine into the organic phase, which can now only diffuse across a shorter distance and still match the mass flux of adipoyl chloride from the opposite side.

This multiscale defect sealing process resulted in a centimeter-scale membrane with a substantial area of monolayer graphene that could isolate two fluid reservoirs with significantly lower leakage than that without defect sealing (Figure 1B−C). After the defect-sealing process, we introduced pores in the graphene by high-energy gallium ion bombardment to nucleate isolated defects followed by etching of the

defects into subnanometer pores using acidic potassium permanganate.[13] The ion energy, angle of incidence, and dose were set at 1 kV, 0°, and $7 \times 10^{13}$ cm$^{-2}$, respectively, which are predicted to yield primarily single vacancy defects at a density of $7 \times 10^{13}$ cm$^{-2}$.[23] Aberration-corrected scanning transmission electron microscopy (STEM) revealed distinct pores and vacancies in graphene (Figure 4A) with a density of $3.89 \times 10^{13}$ cm$^{-2}$ (see Supporting Information Section III.B). Because the atomic size of the carbon atoms in the STEM images is dominated by the size of the electron probe (~1.1 Å at 60 kV), and not by the carbon electronic charge density, the pores appear larger in STEM than their effective size for ion transport. We renormalized the pore size to account for the van der Waals size of the carbon atoms (see Supporting

Information Section III.B). The resulting pore size distribution was log-normal with a mean pore diameter of 0.162 nm and a tail extending a little beyond 0.5 nm (Figure 4B). Given that the van der Waals diameter of a water molecule is 0.275 nm, only the larger pores corresponding to a density of $1.57 \times 10^{12}$ $cm^{-2}$ are expected to be water permeable, and almost all of the pores are expected to be impermeable to salt ions (∼0.7 nm diameter).[3]

We first investigated water transport across the defect-sealed nanoporous graphene membrane under forward osmosis using glycerol ethoxylate (∼1 kDa) as the draw solute. The defect-sealing process resulted in negligible leakage of the draw solute to the opposite side (Supporting Information Figure S5), which is critical for measuring transport across the graphene and also indicates selectivity of the created pores. Water flux across the membrane increased linearly with osmotic pressure of the draw solute and was significantly higher than the water flux in a control experiment where the ion bombardment step was omitted (Figure 4C). Flux across the control membrane is likely a result of some combination of flow across residual defects[13] and the polymer used to seal defects (see Supporting Information Figure S3). The permeance of the membrane, defined as the measured flux of water with respect to the nominal area of the PCTE pores divided by the driving osmotic pressure, was $1.41 \pm 0.23$ and $0.43 \pm 0.06$ L $m^{-2}$ $h^{-1}$ $bar^{-1}$ for the membrane and control, respectively, which is in the same order of magnitude as current reverse osmosis membranes for seawater desalination.[24] From these results, we extracted bounds on the experimentally measured average permeance per graphene pore by accounting for the density of water-permeable pores from the STEM imaging, the actual graphene area, and by subtracting out the permeance of the control (see Supporting Information Section III.D). We arrive at an expected permeance per pore of $1.93$ $(+58.5, -1.02) \times 10^{-8}$ $ns^{-1}$ $Pa^{-1}$ for an average weighted pore size of 0.487 nm, with the uncertainty arising primarily due to difficulty in knowing the actual number of graphene pores that permit transport (see Supporting Information Section III.D). The mean pore size is smaller than the pores studied using molecular dynamics by Cohen-Tanugi et al.[3] but is consistent with molecular dynamics simulations by Suk et al.[10] (Figure 4D) and is fairly close to predictions by continuum models.[10]

Finally, we examined the ability of the nanoporous graphene membrane to reject solutes under forward osmosis. We tested four different solutes: NaCl (0.716 nm size), $MgSO_4$ (0.86 nm size), Allura Red (a model anionic organic molecule of 496 Da and ∼1.0 nm size), and dextran (MW 4.4 kDa and ∼3.7 nm size). The membrane exhibited ∼70% rejection of $MgSO_4$, ∼90% rejection of Allura Red and ∼83% rejection of dextran (Figure 4E). The higher rejection of Allura Red compared to dextran likely arises from electrostatic repulsion between the anionic Allura Red molecule and the negatively charged pores.[13] More interestingly, NaCl exhibited a negative rejection, indicating that the rate at which NaCl transports across the membrane exceeds the transport rate expected for nonselective convective flow. This behavior is observed in nanofiltration when transport by diffusion exceeds that due to convection.[25] This transport of NaCl may be attributed to the few-nanometer scale defects[14] that are too large to be sealed using ALD and too small to allow blocking by interfacial polymerization (see Supporting Information Section III.C), and to the increased permeability of nylon-6,6 to monovalent ions during the etching step of pore creation (see Supporting Information

Figure S3). Regardless, we find that the trends in solute fluxes and rejections can be explained quantitatively for all solutes except NaCl using a continuum model of solute transport (Figure 4E) (see Supporting Information Section III.E for details of the model). The model accounts for diffusion and advection across nanoporous graphene assuming a log-normal pore size distribution and transport in the PCTE membrane pore in series with the graphene. The discrepancy in the case of NaCl is expected given its leakage across nylon-6,6.

This work demonstrates the feasibility of realizing ultrathin nanoporous monolayer graphene membranes for ionic and molecular-level filtration via defect sealing. The experimental approach also presents a platform for studying nanofluidic transport across membranes made from graphene and other ultrathin materials. Advancing graphene membranes for desalination and nanofiltration will require additional effort in optimizing the pore generation and defect sealing processes, manufacturing of the membranes at larger scales, and investigating other factors that impact performance such as biofouling and scaling. Regardless, the experimental results are consistent with theoretical predictions of high flux across graphene pores, indicating their potential to outperform existing membranes for a range of filtration applications in water desalination, nanofiltration, biofiltration, chemical processing, and gas separations.

**Materials and Methods.** Detailed materials and methods are described in the online Supporting Information.

*Materials.* Graphene was grown on copper foil (JX Nippon Mining & Metals HA Foil) in a home-built system using Low-Pressure Chemical Vapor Deposition (LPCVD). First, the copper foil was placed in a quartz tube and annealed at 1000 °C for 30 min in a hydrogen environment. Next, the graphene was grown for 30 min by increasing $H_2$ flow rate to 70 sccm and setting the $CH_4$ flow rate to 0.5 sccm. The chamber pressure during the growth phase was 1.90 Torr. The growth conditions outlined above produce high-quality graphene with very few bilayer regions. Detailed characterization of the graphene is reported in a previous publication.[13]

Copper etchant used for transfers was APS-100 (10−20% ammonium persulfate, Transene). Target substrates for graphene transfers were Sterlitech non-PVP coated, hydrophobic, polycarbonate track etch (PCTE) membranes with 200 nm pores and gold 200 mesh Quantifoil Holey Carbon transmission electron microscope grids (TEM, Ted Pella, Inc.) with 1.2 $\mu$m diameter holes. PCTE surface was modified with didecylamine (Sigma-Aldrich). Monomers used to close defects using interfacial polycondensation were 98% hexamethylenediamine (Sigma-Aldrich) and 98% adipoyl chloride (Sigma-Aldrich). Fluorescent molecule for nylon labeling was Texas Red-X Succinimidyl Ester (Life Technologies). Dyes and salts used in transport experiments were potassium chloride (KCl, Mallinckrodt Chemicals), 98% Allura Red AC (Sigma-Aldrich), sodium chloride (Sigma-Aldrich, Sigma Ultra), and magnesium sulfate (Sigma-Aldrich), and 4.4 kDa tetramethylrhodamine isothiocyanate−dextran (Sigma-Aldrich). Osmotic draw solution used in forward osmosis measurements was 98% glycerol ethoxylate (∼1 kDa, Sigma-Aldrich).

*Experimental Setup for Transport Measurements.* Transport driven by osmotic pressure gradient was measured in a customized 7.0 mL Side-Bi-Side glass diffusion cell with a 5.5 mm orifice (Permegear, Inc.). A 250 $\mu$L graduated syringe (Hamilton Gastight 1725) was inserted into an open port of the cell and sealed with wax for leak-free connection (see

Supporting Information Figure S1). Depending on which side the draw solution was placed, a rise/drop of liquid meniscus level along the graduated syringe took place as the fluid was transported to the draw side. The meniscus displacement was recorded with a digital camera every minute over the course of measurement. Each experiment was repeated three times by replenishing with new solution to quantify the uncertainty in measurement.

*Water Transport Measurements.* Water transport experiments were carried out with degassed deionized (DI) water as the feed solution and draw solutions of glycerol ethoxylate (Sigma-Aldrich) with average molecular weight $M_n \sim 1,000$. The syringeless side (feed side) was filled with 7.25 mL of DI water and the syringe side (graphene side) was filled with 7.4 mL of 11.49−29.68 wt % glycerol ethoxylate solution (see Supporting Information Table S1) and then sealed by a rubber plug, thereby imposing ~5−25 atm (~0.5−2.5 × 10^6 Pa) osmotic pressure gradient across the membrane (Supporting Information Figure S1−a). Transport of water was driven from the feed side to the draw side by the osmotic gradient that resulted in a rise of water meniscus along the syringe. After measuring the displacement of the meniscus for 20 min, the solution in each side of the cell was replaced and the measurement procedure was repeated.

*Salt Transport Measurements.* Osmotically driven salt transport measurements were performed with 16.6 mM NaCl (Sigma-Aldrich) solution and 16.6 mM MgSO$_4$ (Sigma-Aldrich) solution, both in degassed DI water. The syringeless side (draw side) was filled with 7.25 mL of 26.47 wt % glycerol ethoxylate solution and the syringe side (feed side) was filled with 7.4 mL of each salt solution and then sealed with a rubber plug (see Supporting Information Figure S1). Introducing the solute on the graphene side ensured minimal concentration polarization that would otherwise occur within the unstirred PCTE membrane pores. An eDAQ Conductivity Isopod with a Miniature Dip-In Conductivity Electrode (eDAQ Inc.) was immersed in the draw solution and measured the rise in conductivity every 15 s for 15 min. The cell constant of the conductivity electrode was calculated with respect to a 0.5 mS/cm standard KCl solution (Sigma-Aldrich) prior to and immediately following each experiment. The properties of the salts investigated are provided in Supporting Information Table S2.

*Organic Molecule Transport Measurements.* Osmotically driven organic molecule transport was carried out with 1.3 mM Allura Red AC (Sigma-Aldrich) solution and 1 mM 4.4 kDa tetramethylrhodamine isothiocyanate−dextran (TMRD, Sigma-Aldrich) solution, both in degassed DI water. As in the salt transport experiments, the syringeless side (draw side) was filled with 7.25 mL of 26.47 wt % glycerol ethoxylate solution and the other side (feed side) was filled with 7.4 mL of each organic molecule solution and then sealed with a rubber plug. A fiber optic dip probe attached to a Cary 60 UV−vis Spectrophotometer was immersed in the draw side to measure the change in absorbance spectrum from 190 to 1100 nm every 15 s for 40 min in case of Allura Red AC and every 3 min for 480 min in the case of the TMRD. To account for possible shifts of absorbance curves over the course of measurement, the difference was taken between the local peak emerging from the rise in organic molecule concentration and a point independent of concentration, instead of using the absolute measured values. The absorbance peaks for Allura Red AC and TMRD occurred at 510 and 520 nm, respectively, whereas the concentration-

independent points were at 710 nm for both molecules. The properties of the organic molecules are presented in Supporting Information Table S2.

## ■ ASSOCIATED CONTENT

### Ⓢ Supporting Information

Materials and methods, data analysis, and theoretical models. This material is available free of charge via the Internet at http://pubs.acs.org.

## ■ AUTHOR INFORMATION

### Corresponding Author
*E-mail: karnik@mit.edu.

### Notes
The authors declare the following competing financial interest(s): R.K. discloses financial interest in a company that aims to commercialize graphene membranes.

## ■ ACKNOWLEDGMENTS

## ■ REFERENCES

(1) Service, R. F. *Science* **2006**, *313*, 1088−1090.
(2) Miller, J. *Review of Water Resources and Desalination Technologies*; Sandia National Laboratories: Albuquerque, NM, 2003.
(3) Cohen-Tanugi, D.; Grossman, J. *Nano Lett.* **2012**, *12*, 3602−3608.
(4) Gai, J. G.; Gong, X. L.; Wang, W. W.; Zhang, X.; Kang, W. L. *J. Mater. Chem. A* **2014**, *2*, 4023−4028.
(5) Cohen-Tanugi, D.; Grossman, J. *J. Chem. Phys.* **2014**, *141*, 074704.
(6) Humplik, T.; et al. *Nanotechnology* **2011**, *22*, 292001.
(7) Lee, C.; Wei, X.; Kysar, J. W.; Hone, J. *Science* **2008**, *321*, 385−388.
(8) Bunch, J. S.; et al. *Nano Lett.* **2008**, *8*, 2458−2462.
(9) Suk, M. E.; Aluru, N. R. *J. Phys. Chem. Lett.* **2010**, *1*, 1590−1594.
(10) Suk, M. E.; Aluru, N. R. *RSC Adv.* **2013**, *3*, 9365−9372.
(11) Suk, M. E.; Aluru, N. R. *J. Chem. Phys.* **2014**, *140*, 084707.
(12) Boutilier, M. S. H.; et al. *ACS Nano* **2014**, *8*, 841−849.
(13) O'Hern, S. C.; et al. *Nano Lett.* **2014**, *14*, 1234−1241.
(14) O'Hern, S. C.; et al. *ACS Nano* **2012**, *6*, 10130−10138.

(15) Koenig, S.; Wang, L.; Pellegrino, J.; Bunch, J. S. *Nat. Nanotechnol.* **2012**, *7*, 728−732.

(16) Celebi, K.; et al. *Science* **2014**, *344*, 289−292.

(17) Lee, J. H.; et al. *Science* **2014**, *344*, 286−289.

(18) Wang, X.; Tabakman, S. M.; Dai, H. *J. Am. Chem. Soc.* **2008**, *130*, 8152−8153.

(19) Sun, X.; et al. *J. Electrochem. Soc.* **2012**, *159*, A364−A369.

(20) Blanc, P.; Larbot, A.; Palmeri, J.; Lopez, M.; Cot, L. *J. Membr. Sci.* **1998**, *149*, 151−161.

(21) Wittbecker, E.; Morgan, P. *J. Polym. Sci., Part A: Polym. Chem.* **1996**, *34*, 521−529.

(22) Morgan, P.; Kwolek, S. *J. Polym. Sci., Part A: Polym. Chem.* **1996**, *34*, 531−559.

(23) Lehtinen, O.; Kotakoski, J.; Krasheninnikov, A.; Keinonen, J. *Nanotechnology* **2011**, *22*, 17.

(24) Pendergast, M. M.; Hoek, E. M. V. *Ener. Environ. Sci.* **2011**, *4*, 1946−1971.

(25) Gilron, J.; Gara, N.; Kedem, O. *J. Membr. Sci.* **2001**, *185*, 223−236.